RSC Advances

ROYAL SOCIETY OF CHEMISTRY

www.rsc.org/advances

Cite this: DOI: 10.1039/c0xx00000x

www.rsc.org/xxxxxx

ARTICLE

A rhodamine derivative as a highly sensitive chemosensor for Iron(III)

Kaitian Wu[a], Hongde Xiao[a], Lele Wang[b], Gui Yin[a*], Yiwu Quan[a], and Ruiyong Wang[b*]

Received (in XXX, XXX) Xth XXXXXXXXX 20XX, Accepted Xth XXXXXXXXX 20XX
DOI: 10.1039/b000000x

A novel rhodamine-based fluorescent probe **P1** was synthesized, which was developed for optical detection of Fe^{3+}. Compared with other commonly coexistent metal ions in aqueous system, it exhibited high sensitivity and selectivity for Fe^{3+}. The detection limit was only 0.1 μM with fluorescence experiment. The rapid enhancement of fluorescence intensity on addition of Fe^{3+} provided a good method of detection for Fe^{3+}. The color change was visible and distinct, so it could be used for naked-eye detection. Furthermore, this fluorescent probe was proved effective when used for detecting Fe^{3+} in living cells and zebrafish. This showed its values in biological aspects.

1. Introduction

Metal ions play important roles not only in chemical reactions but also in a lot of biological processes. They are indispensible in our daily life[1,2]. As a result, it is quite necessary to find efficient ways to detect different ions electively and sensitively. The fluorescent probes have been designed and synthesized to meet the above acquirements[3-5]. Fluorescent chemosensors now are widely used in medical, environmental and biological applications[6,7]. They can show scientists molecular details of biological processes involved with the change of metal ions[8,9]. The chemosensors can make it possible for remote measurement, for which reason people don't need to worry about damaging the samples or removing them from their natural medium[10]. For the above reasons, the development of elective and sensitive chemosensors has drawn a great deal of attention [11].

As one of the most essential trace elements in biological system, iron plays indispensible roles in growth and development of living systems as well as in quite a number of cellular biochemical processes[12]. It provides the oxygen carrying capacity of heme around the body. It is also crucial in cellular metabolism and enzymatic reactions[13]. Although it's quite important in living systems, its deficiency and overdose can induce serious biological disorders[14]. Iron deficiency will lead to anemia, low blood pressure and hypoimmunity because of the difficulties in oxygen delivery of cells. Conversely, the overload of iron in living systems can result in reactive oxygen species (ROS) through Fenton reaction. As a result, the lipids, nucleic acids, and proteins are damaged greatly[15]. Several diseases, such as such as Alzheimer's, Huntington's, and Parkinson's diseases, have already been proved to be connected with the cellular toxicity[16-18]. Thus, reliable methods of quantification detection are badly needed in clinical, medicinal, environmental and industrial aspects[19]. Because of the easy monitoring, low cost, high sensitivity, good selectivity, high level of biosecurity and the rapid enhancement of the fluorescence intensity, chemosensor is a good choice to detect Fe^{3+} and great contributions to the development of fluorescent detection for Fe^{3+} have been made in the past decades. As we know, the rhodamine with spirolactam structure is colorless and non-fluorescent, whereas ring-opening of the spirolactam induced by the analyte gives rise to pink color and a strong fluorescence emission. Moreover, rhodamine has a longer emission wavelength and high fluorescence quantum yield, which is suitable for detecting ions in living cells. So far, a number of fluorescent probes for Fe^{3+} have been reported [20, 21] but only a few of them are satisfying. Other transition-metal ions, such as Cu^{2+}, Co^{2+}, Cr^{3+}, Pb^{2+}, Hg^{2+}, can easily interfere the Fe^{3+}, resulting in bad selectivity and sensitivity[22]. Many of the probes cannot be used in living cells because of their cellular toxicity. What's more, most of the probes are prone to be influenced by the background fluorescence because they have a shorter emission wavelength (below 500 nm). Colour change cannot be identified by the naked eye, either[23-25]. Many of them are incompatible with aqueous environments, restricting their applications in life [11].

In this work, we developed and synthesized a based-on rhodamine fluorescent probe **P1**. It has high sensitivity and selectivity, and the enhancement of the fluorescent intensity is rapid. It is compatible with aqueous environments well. Strong yellow fluorescence can be observed under the excitation at 557

[a]*State Key Laboratory of Analytical Chemistry for Life Science, School of Chemistryand Chemical Engineering, Nanjing University, Nanjing 210093, People's Republicof China. E-mail: yingui@nju.edu.cn*
[b] *State Key Laboratory of Pharmaceutical Biotechnology; School of Life Science, Nanjing University, Nanjing, 210093, People's Republic of China. E-mail: wangry@nju.edu.cn*
[c]*Jiangsu Key Laboratory of Advanced Catalytic Materials and Technology, Changzhou University, 213164, China*

† Electronic supplementary information (ESI) available. See DOI: 10.1039/

nm. What's more, the color changes from yellow to deep pink quickly and obviously after adding Fe^{3+} in **P1**. In the fluorescence titration experiments, the fluorescence intensity remains unchanged after the concentration of the Fe^{3+} is more than 1 equiv. what's more, the biological experiment proves that **P1** could act well in living cells, showing its practical and wide range of applications.

2. Experimental

2.1. Materials and Apparatus

All of the chemicals were from commercial suppliers. The solvents (methanol, ethanol) were dried and distilled before we used them. All of the other chemicals were of analytical reagent grade, unless otherwise referred to. As for the aqueous solutions, the water was purified by Milli Q Advantage Water Purification System. ^{1}H NMR and ^{13}C-NMR spectra were recorded using a Bruker Ultrashield 300MHz spectrometer operating at 300 and 75 MHz, respectively. They were in deuterated dimethyl sulphoxide (DMSO-d_6) as the solvent. Chemical shifts were expressed in ppm and TMS was the internal standard. Mass spectroscopy was carried out by Micromass GC-TOF and Agilent Technologies 6540 UHD Accurate-Mass Q-TOF LC/MS instruments. Hitachi Fluorescence spectrophotometer-F-4600 was used to measure fluorescence spectra. Varian Cary 50 Probe UV/Vis spectrophotometer was used to measure UV/Vis spectra. Olympus FV-1000 laser scanning confocal fluorescence microscope was used to capture with fluorescent images.

2.2. Intermediates and Monomer Synthesis

The overall synthetic steps for the monomer were shown in Scheme 1.

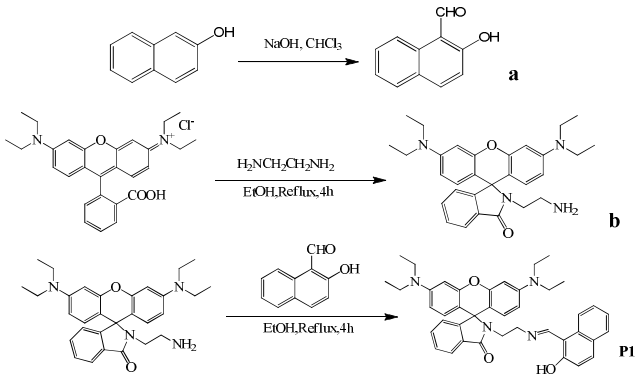

Scheme 1. Schematic of **P1** synthesis

*Synthesis of compound **a***. Compound **a** was synthesized according to an article earlier reported [26].

*Synthesis of compound **b***. Rhodamine B (4.79 g, 10 mmol) in ethanol solution (30 mL) in a 100-mL round-bottomed flask was added ethylenediamine (10mL). The solution was heated at reflux and stirred for 4 h. After cooling to room temperature, a red solid precipitated and was washed by cool ethanol until the filtrate turned colorless.^{1}H-NMR (300 MHz, DMSO, 25 ℃): δ = 7.75 （s, 1H）, 7.47 (s, 2H), 6.98 (s, 1H), 6.33 (d, 6H, *J*=9.0 Hz), 3.31 (d, 8H, *J* = 6.0 Hz), 2.94 (d, 2H, *J* = 9.0 Hz), 2.18 (d, 2H, *J* = 6.0Hz), 1.07 (t, 12H, *J* = 6.0Hz) ESI-MS: m/z = 485.20 $[M+H]^+$

*Synthesis of compound **P1***. Compound b (1.21 g, 2.5 mmol) in ethanol solution (25 mL) in a 100-mL round-bottomed flask was added compound **a** (0.43g, 2.5mmol). The solution was then heated at reflux for overnight. After cooling to room temperature, yellow solid precipitated out. The solid was washed by cool ethanol until the filtrate turned colourless, then we made the solid dried in vacuo. Yield: 1.12 g (70 %), yellow powder **P1**. ^{1}H-NMR (300 MHz, DMSO, 25 °C): δ = 13.84 (s, 1 H), 8.75 (d, 1 H, *J* = 8.5Hz), 7.38-7.90 (m, 6 H), 7.16 (s, 1H,), 7.01 (s, 1H), 6.69 (d, 2 H, *J* = 9.2Hz), 6.29 (dd, 5 H, *J* = 6.0, 6.0Hz), 3.42 (s, 4 H), 3.22 (d, 8 H, *J* = 5.7 Hz), 1.02 (s, 12 H) ppm. ^{13}C-NMR (75 MHz, DMSO, 25 °C): δ = 176.42, 167.99, 159.71, 153.94, 153.08, 148.83, 137.21, 134.49, 133.29, 130.57, 129.28, 128.78, 128.65, 128.21, 125.80, 125.42, 124.09, 122.90, 122.64, 118.81, 108.62, 106.59, 105.19, 97.70, 64.64, 49.70, 44.08, 40.99, 12.79 ppm. ESI-MS: m/z = 639.30$[M+H]^+$ 661.30$[M+Na]^+$ 677.25$[M+K]^+$.

2.3. Measurement Procedures

Stock solutions of 1.0×10^{-3} M **P1** and 1.0×10^{-3} M Fe^{3+} were prepared by dissolving **P1** in ethanol-H_2O (1:1) solution and $Fe_2(SO_4)_3$•$9H_2O$ in doubly distilled water, respectively. The Fe^{3+} solution was diluted stepwise to yield working solutions with concentrations ranging from 0.1 μM to 5 μM. The pH range solutions were prepared by adjusting 50 mM Tris–HCl solution with HCl or NaOH solution. Solutions of the other metal ions were prepared by dissolving $Al(NO_3)_3$•H_2O, $LiClO_4$, NaCl, KCl, $MgCl_2$, $CaCl_2$, $Fe(NO_3)_2$•$6H_2O$, $FeCl_3$•$6H_2O$, $CoCl_2$•$6H_2O$, $Ni(NO_3)_2$•$6H_2O$, $AgBF_4$, $Cr(NO_3)_3$•$9H_2O$, $Cd(NO_3)_2$•$4H_2O$, $ZnCl_2$, $Hg(ClO_4)_2$•$3H_2O$, $CuCl_2$•$2H_2O$, $Pb(NO_3)_2$, $Mn(NO_3)_2$, $GaCl_3$, $FeSO_4$•$7H_2O$ and $HgCl_2$ in doubly distilled water (1.0×10^{-3} μM).

2.4. Cell imaging

A fresh stock of HeLa cells was seeded into a glass bottom dish with the density of 1×10^{-5} cells per dish, incubated for 24 h. Then, 10 μM compound **P1** (198 mL DMEM mixed with 2 mL of 1.0×10^{-3} M **P1** solution in ethanol-H_2O) solution is added to the cell for 15 min at room temperature. Then the solution was removed and the cells were washed by PBS (2 mL, 3 times) to clear the **P1** molecules which did not get inside the cells. Afterwards, 10 μM Fe^{3+} DMEM solution was added to the cells，then incubated the cells for 15 min at room temperature. The solution was removed and the cells were washed by PBS (2 mL, 3 times). Fluorescence imaging was performed by confocal laser scanning microscopy (λ_{ex} =546 nm, fluorescent signals were collected at 550-650 nm). The images were captured by photomultiplier.

2.5. Fluorescent imaging of Fe^{3+} in zebrafish

Zebrafish were raised at 28℃ and maintained at optimal breeding conditions. For mating, male and female zebrafish were maintained in one tank at 28℃ on a 12-h light/12-h dark cycle, and then the spawning of eggs was triggered by giving light

stimulation in the morning. Almost all eggs were fertilized immediately. All stages of zebrafish were maintained in E3 embryo media (15 mM NaCl, 0.5 mM KCl, 1 mM $MgSO_4$,1 mM $CaCl_2$, 0.15m M KH_2PO_4, 0.05 mM Na_2HPO_4, 0.7 mM $NaHCO_3$, 5-10% methylene blue; pH 7.5). For imaging experiment, five-day-old zebrafish were incubated with 10 μM BAN solutionfor 20 min at room temperature. The solution was then removed, and the cells were washed with PBS (2 mL×3) to clear BAN molecules attached to the surface of zebrafish. Afterwards, the zebrafish were incubated for 20 min with 40 μM $FeCl_3$ DMEM solution at room temperature. The culture medium was removed, and the treated cells were rinsed three times with PBS (2 mL×3) before observation. The treated zebrafish were imaged by confocal microscopy. All experiments were performed in compliance with Regulations for the Administration of Affairs Concerning Experimental Animals published by Brueau of Legislative Affairs of the State Counsil of People's Republic of China and guidelines of State Key Laboratory of Pharmaceutical Biotechnology in Nanjing university, as well as that the institutional committee (s) have approved the experiments.

3. Results and Discussion

3.1. Fluorescence and visible light response of compound P1 to different metal ions

The various metal ions (Fe^{3+}, Ag^{+}, Al^{3+}, Ca^{2+}, Cd^{2+}, Co^{2+}, Cu^{2+}, Cr^{3+}, Fe^{2+}, Ga^{3+}, Hg^{2+}, K^{+}, Li^{+}, Mg^{2+}, Mn^{2+}, Na^{+}, Ni^{+}, Pb^{2+}, Zn^{2+}) were used to evaluate the metal-ion bonding property and selectivity of the probe **P1** in aqueous solution. When 10 equiv. of these metal ions were added to 50 μM ethanol–Tris–HCl buffer (v/v, 1/9, pH = 7.0) solutions of **P1**, the Fe^{3+} and Hg^{2+} induced color change from yellow to pink, but the color change that Hg^{2+} causes was very weak (Fig 1). With a hand-held UV lamp (at the excitation 365 nm), we could see that both Fe^{3+} and Hg^{2+} induced fluorescence enhancement, but Hg^{2+} could only cause very weak fluorescence enhancement (Fig 2). In addition of Fe^{3+} and Hg^{2+}, other ions could not cause color change or fluorescence change.

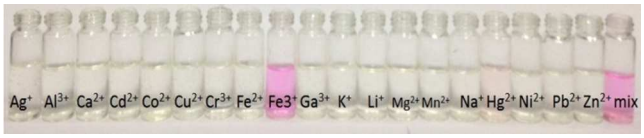

Fig 1. Changes in the visible light of **P1** (50 μM) in ethanol–Tris–HCl buffer (v/v, 1/9, pH = 7.0) solutions upon addition of various metal ions (10equiv.). Mix means **P1** with all kinds of metal ions.

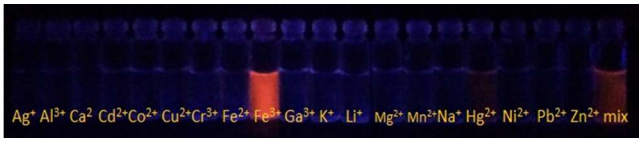

Fig 2. Changes in the fluorescence of **P1** (50 μM) in ethanol–Tris–HCl buffer (v/v, 1/9, pH = 7.0) solutions upon addition of various metal ions (10 equiv.) under excitation at 365 nm (with a hand-held UV lamp).Mix means **P1** with all kinds of metal ions.

Fig 3 showed the UV-Vis absorption spectra of **P1** upon addition of the various metal ions. The results showed that the color change was distinct after adding Fe^{3+} into **P1**. Although Hg^{2+} could induce color change, the color change was not as obvious as Fe^{3+}.

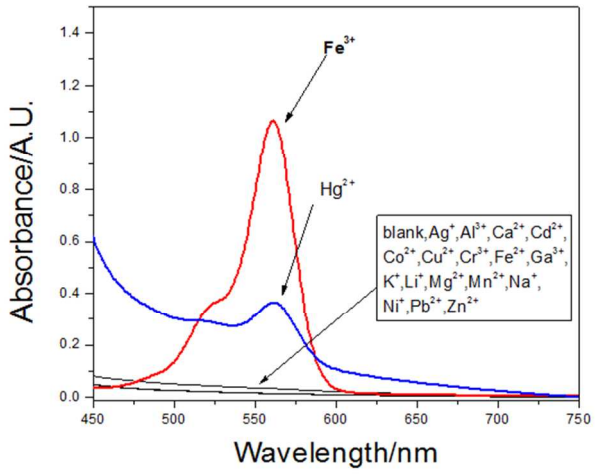

Fig 3. Absorption spectra of **P1** (100μM) in ethanol–Tris–HCl buffer (v/v, 1/9, pH = 7.0) with the presence of 1equiv. of different metal ions.

Fig 4 showed the fluorescence spectra of **P1** upon addition of the various ions. **P1** showed no fluorescence upon excitation at 557 nm. Fe^{3+} induced a great increase in fluorescence intensity. One emission peak at 581.5 nm could be detected. Hg^{2+} could also induce increase in fluorescence intensity with the emission peak at 587nm, but the fluorescence intensity was far weaker than Fe^{3+}. So, the 5nm red shift of the emission peaks between Fe^{3+} and Hg^{2+} and the different fluorescence intensity changes made it possible for the **P1** to discriminate between Fe^{3+} and Hg^{2+}.

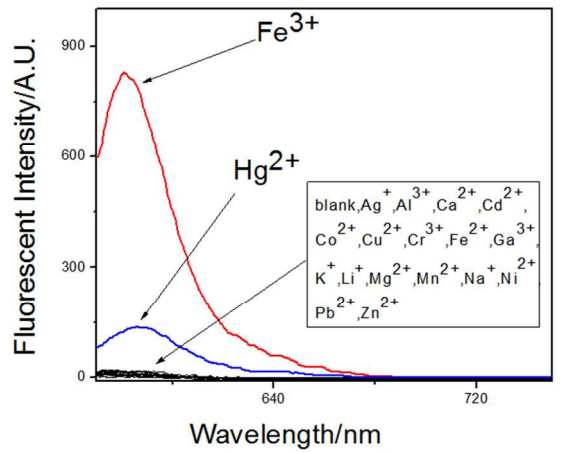

Fig 4. Fluorescence spectra of **P1** (5 μM) in ethanol–Tris–HCl buffer (v/v, 1/9, pH = 7.0) with the presence of 1equiv. of different metal ions upon excitation at 557 nm.

3.2. Competition experiment

To prove that the selectivity for Fe^{3+} is good in a complex background of all kinds of metal ions, the fluorescence intensity enhancement of **P1** with Fe^{3+} was detected in the presence of the

potentially competing metal ions. One equiv. of Fe^{3+} was added into **P1** in the presence of the various metal ions (K^+, Na^+, Ca^{2+} were 50 equiv., others were 10 equiv.). From Fig 5, we could see that the fluorescence intensity enhancement caused by Fe^{3+} stayed unchanged after adding all the other kinds of metal ions. 10 equiv. of Hg^{2+} could not influence the detection of Fe^{3+}. The phenomenon that 50 equiv. of K^+, Na^+, Ca^{2+} could not influence the fluorescence intensity enhancement proves that probe **P1** may perform well in living cells where the ions K^+, Na^+, Ca^{2+} are active.

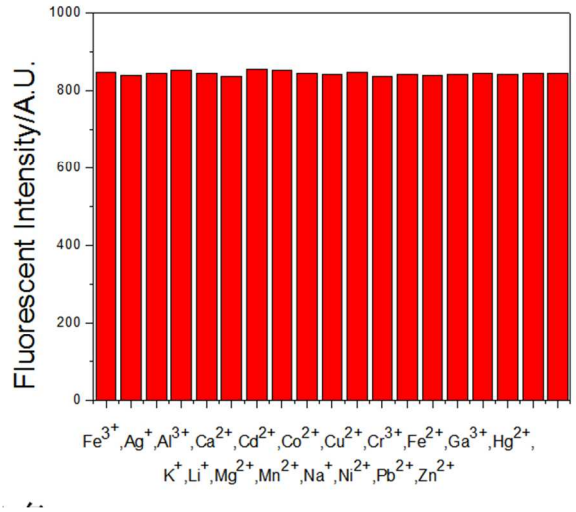

Fig 5. Competition experiment of **P1** towards Fe^{3+} (1 equiv.) in the absence or presence of various metal ions (K+, Na+, Ca^{2+} were 50 equiv., others were 10 equiv.). Excitation wavelength is 557 nm, emission wavelength is 581.5 nm.

3.3. UV-Vis measurement

Fig 6 showed the quantitative UV-Vis absorption spectra of **P1**. Different concentrations of Fe^{3+} from 0.1~1 equiv. were added into 100 μM of **P1** in ethanol–Tris–HCl buffer (v/v, 1/9, pH = 7.0) solution. The absorption increased with concentrations of Fe^{3+} and the pink color became deeper, which could be ascribed to structure variation of **P1** from a spirocyclic form to a ring-opened amide form.

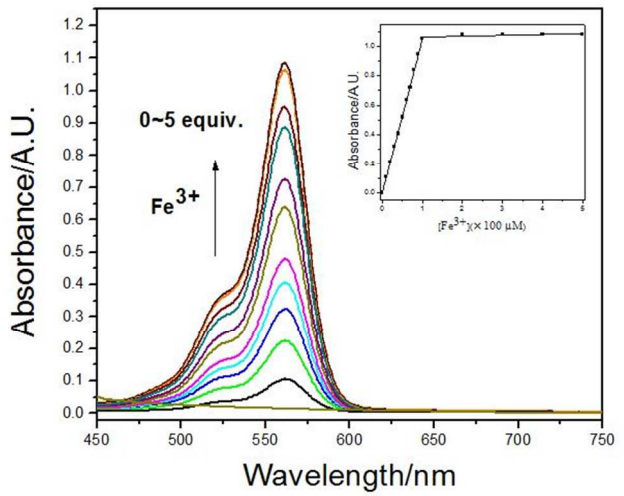

Fig 6. Absorption spectra of **P1** (100 μM) in ethanol–Tris–HCl buffer(v/v, 1/9, pH = 7.0) solution with the presence of different concentrations of Fe^{3+} (0, 0.1, 0.2, 0.3, 0.4, 0.5, 0.6, 0.7, 0.8, 0.9, 1.0 equiv.).

The molar absorptivity was calculated to be 1.05×10^4 L • mol^{-1} • cm^{-1}. From the absorption titrations, the association constant of **P1** with Fe^{3+} was calculated to be 9.31×10^{-5} (R = 0.9998) by using nonlinear least-square analysis (Fig 7). This experiment proved that the detection limit of Fe3+ is 1.7 μM.

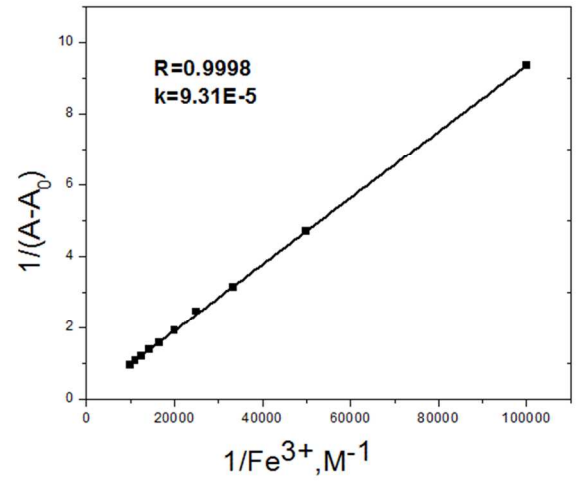

Fig 7. The association constant of **P1** to Fe^{3+} in ethanol–Tris–HCl buffer (v/v, 1/9, pH =7.0) solution. The concentration of **P1** is kept at 100 μM.

3.4. Fluorescence measurement

Fig 8 showed the quantitative fluorescence spectra of **P1** on addition of different concentrations of Fe^{3+} from 0~5 equiv in ethanol–Tris–HCl buffer (v/v, 1/9, pH = 7.0) solution. With the increase of the concentration of Fe^{3+}, the fluorescence intensity increased proportionally. When the concentration of Fe^{3+} increased up to 1 equiv. of **P1**, the fluorescence intensity stayed unchanged.

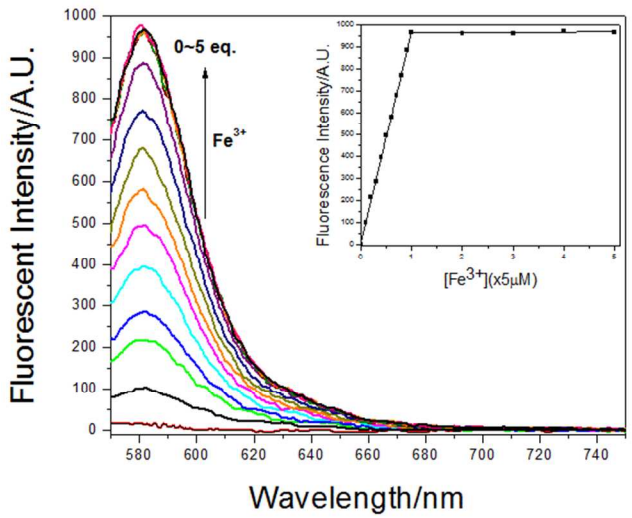

Fig 8. Fluorescence spectra of **P1** (5 μM) in ethanol–Tris–HCl buffer(v/v, 1/9, pH = 7.0) solution with the presence of different concentrations of Fe^{3+} (0, 0.1, 0.2, 0.3, 0.4, 0.5, 0.6, 0.7, 0.8, 0.9, 1.0, 1.5, 2.0, 2.5, 3.0,4.0, 5.0 equiv.) upon excitation at 557 nm. Insert: fluorescence intensity changes at 581.5 nm.

Fig 9 showed the detection limit of the probe **P1**with Fe^{3+}. The concentration of **P1** was 1μM and the concentrations of Fe^{3+} increased from 0~1 equiv. of **P1**. This experiment proved that the detection limit of Fe^{3+} is 0.1 μM.

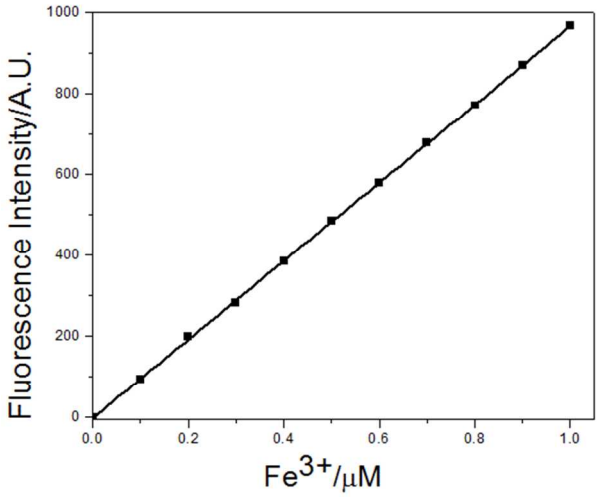

Fig 9. Fluorescence intensities at 581.5 nm of **P1** (1 μM) in ethanol–Tris–HCl buffer (v/v, 1/9, pH = 7.0) solution as a function of [Fe^{3+}]. The excitation wavelength is 557 nm and the observed wavelength is 581.5 nm.

3.5. pH effect

To examine the application of the probe **P1**, the effect of pH experiment was conducted. As was shown in Fig 10, probe **P1** exhibited no fluorescence in the solution of 2~12 pH. The fluorescence intensity of **P1** in presence of 1 equiv. Fe^{3+} in strongly acidic environment was not as strong as in weakly acidic environment. The fluorescence intensity increased from pH 3~4. A portion of **P1** might decompose in strongly acidic environment. With the pH range of 4~7, the fluorescence intensity stayed strongest and unchanged. But as the alkalinity increased, the fluorescence intensity decreased rapidly because Fe^{3+} existed in the form of $Fe(OH)_3$, decreasing the quantity of Fe^{3+} in solution. The fluorescence could not be detected when pH was up to 7.5. Another experiment had been conducted to prove that the vanishment of the fluorescence was caused by the existence of $Fe(OH)_3$. **P1** was kept in solution (pH=7.2 and 12.0) for 24 hours, and no new compound was detected by the way of thin-layer chromatography (TLC) [27]. That proved probe **P1** was stable in alkaline condition and the existence of $Fe(OH)_3$ made the fluorescence intensity decrease rapidly.

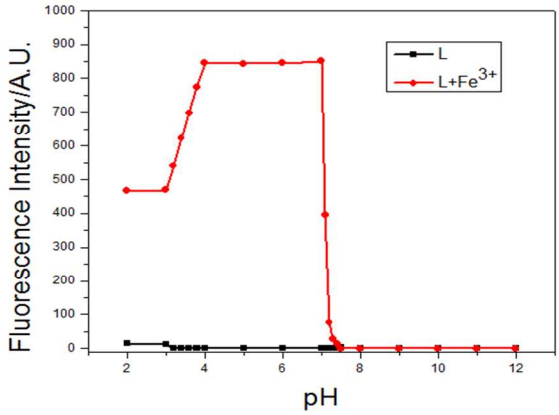

Fig 10. Fluorescence intensity of **P1** (5 μM) at various pH values in ethanol–Tris–HCl buffer (v/v, 1/9, pH = 7.0) solution, in the absence and presence of Fe^{3+} (1 equiv.). Excitation wavelength is 557 nm, emission wavelength is 581.5 nm.

3.6. Investigation of the binding mode

The Job plot experiment was carried out to study the binding stoichiometry between Fe^{3+} and **P1**. In this experiment, the total concentration of **P1** and Fe^{3+} was kept unchanged to be 10 μM while the concentration of Fe^{3+} increased from 0 μM to 10 μM (Fig 11). The fluorescence intensity became strongest when the molar fraction of Fe^{3+} was 0.5, which implied that the binding stoichiometry between Fe^{3+} and **P1** is 1 : 1. In addition, in the ESI-MS spectrum of **P1** in the presence of Fe^{3+} (Fig S1), the peak was at 725.25 (calculated value is 725.28), which was assigned to [**P1**+Fe^{3+}+CH_3OH-$2H^+$]$^+$. That confirmed a 1 : 1 stoichiometry for the **P1**–Fe^{3+} complex. The proposed structure of the **P1**–Fe^{3+} complex was shown in Scheme 2. [21] The binding mechanism of P1 and Fe3+ was further investigated by FT-IR spectroscopy (Fig. S7). The results showed the comparison of the FT-IR spectra of P1 and P1+Fe3+, the characteristic absorption peak of C=O with λmax=1688 cm−1 in the central spirolactam of P1 disappears and shift to 1637 cm-1 after addition of Fe3+, indicating that oxygen atom in the carbonyl group do participate in the coordination. In addition, signals in the region of 1000–1500 cm−1 assigned to stretching vibration C-N and C-O moved to high frequency. This could be attributed to coordination of the nitrogen and oxygen atoms.

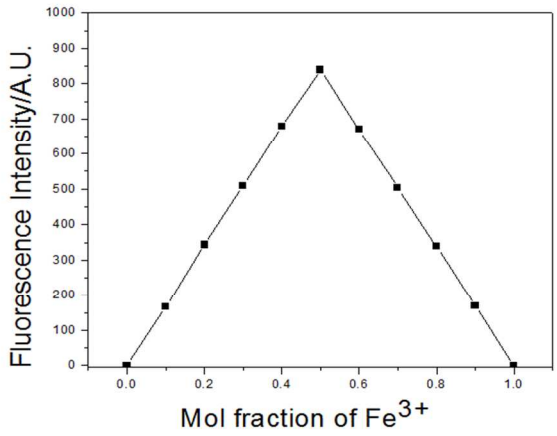

Fig 11. Job plot of the **P1**–Fe^{3+} complexes in ethanol–Tris–HCl buffer(v/v, 1/9, pH = 7.0) solution, keeping the total concentration of **P1** and Fe^{3+} at 10 μM. The observed wavelength is 581.5 nm.

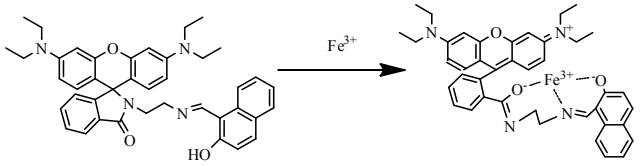

Scheme 2. Proposed mechanism for the fluorescence changes of **P1** on the addition of Fe^{3+}

3.7. Imaging of intracellular Fe^{3+}

When HeLa cells were incubated with **P1** (10 μM) for 15 min at room temperature, nearly no fluorescence could be observed (Fig 12a.). After the treated cells were incubated with Fe^{3+} (10 μM) in the culture medium for 15 min at room temperature, bright red fluorescence could be observed in the HeLa cells(Fig 12d.). The cell morphology remained in good condition after **P1** get inside the cells, indicating good cytocompatibility and low toxicity of the probe. As a result, it could be applied in the detection of Fe^{3+} inside living cells.

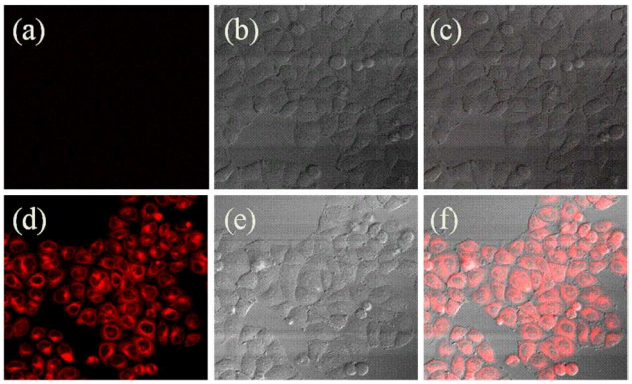

Fig 12. Confocal fluorescence and brightfield images of HeLa cells: (a) Fluorescent image, (b) bright field image and (c) merged image of HeLa cells incubated with the **P1** (10 μM) for 15 min. (d) Fluorescent image, (e) bright field image and (f) merged image of HeLa cells incubated with Fe^{3+} (10 μM) for 20 min after treating with **P1** (λex = 546 nm, fluorescent signals were collected at 550-650 nm).

3.8. Detecting Fe^{3+} in living zebrafish

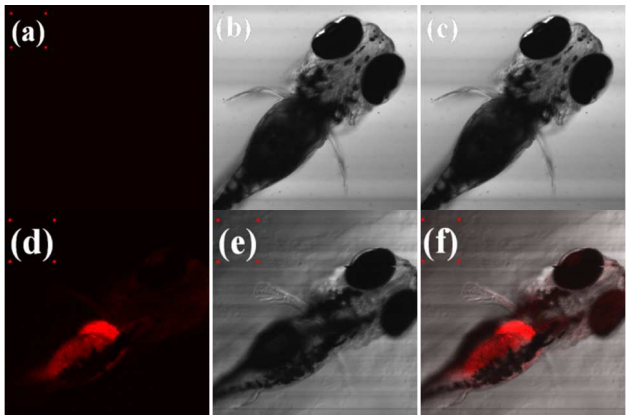

Fig. 13 Fluorescence images of Fe^{3+} in zebrafish using probe **P1** upon excitation at 546 nm. (a)Fluorescent image, (b) bright field image and (c) merged image of zebrafish incubated with probe **P1** (20 μM) for 40 min. (d) Fluorescent image, (e) bright field image and (f) merged image of **P1**-loaded zebrafish incubated with Fe^{3+} (40 μM) for 40 min.

We further employed **P1** in imaging Fe^{3+} in living zebrafish. As shown in Fig. 13, five-day-old zebrafish, treated with probe BAN (10 μM) for 20 min at room temperature, showed very weak fluorescence (Fig. 13a). Moreover, the **P1**-loaded zebrafish treated with 40μM Fe^{3+} give a strong green fluorescence (Fig. 13d). These *in vivo* studies indicated that probe **P1** is suited for monitoring the distribution of Fe^{3+} in living bodies.

Conclusions

In conclusion, we designed and synthesized a new rhodamine-based compound P1. It was highly sensitive and selective for Fe^{3+}. It had fluorescence enhancement and the color change was visible after adding Fe^{3+} in it. The excitation wavelength was 557 nm and the emission wavelength was 581.5 nm. The detection limit of the probe **P1** with Fe^{3+} was 0.1 μM, which showed its good sensitivity. The experiment for cell imaging proved its good cytocompatibility and low toxicity, which meant it could be used for detection of Fe^{3+} inside living cells.

Acknowledgments

We thank the National Natural Science Foundation of China (No.21174061) , National Basic Research Program of China (No. 2014CB846004) , Jiangsu Key Laboratory of Advanced Catalytic Materials and Technology (No. BM2012110) and Jiangsu Province Science Technology Innovation and Achievements Transformation Special Fund (BY2012149).

References

1. B. Valeur, I. Leray. *Coord. Chem. Rev.* 1999, 205, 7-14.
2. Q. Maa, X. Zhang, X. Zhao. *Anal. Chim. Acta.* 2010, 663, 85-87.
3. M. Vonlanthen, N. Finney. *J. Org. Chem.* 2013, 78, 3980-3985.
4. V. A. Babain1, A. V. Legin, D.O.Kirsanov. *Radiochim. Acta.* 2009, 97, 479-484.
5. H. Hisamoto, H. Tohma, T. Yamada. *Anal. Chim. Acta.* 1998, 373, 271-273.
6. Z. Li, K. Li, H. Zhan. *Biochem. Eng. J.* 2012, 11, 2-10.

7. H. N. Kim, M. H. Lee, H. J. Kim. *Chem. Soc. Rev.* 2008, 37, 1465-1472.
8. D. P. Kennedy, C. D. Incarvito, S. C. Burdette. *Inorg. Chem.* 2010, 49, 916–923.
9. H. Wang, D. Wang, Q. Wang. *Org. Biomol. Chem.* 2010, 8, 1017–1026.
10. M. H. Noir, B. Dureault. *Sens. Actuators, B.* 1995, 29, 386-391.
11. K. Moon, Y. Yang, S. Ji, J. Tae. *Tetrahedron Lett*. 2010, 51, 3290-3293.
12. R. R. Crichton, D. T. Dexter, R. J. Ward. *Coord. Chem. Rev.* 2008, 1189-1199.
13. C. Li, C. Zou, Y. Li. *Dyes and Pig.* 2014, 104, 110-115.
14. J. Wang, D. Zhang, Y. Liua, P. Dinga. *Sens. Actuators, B.* 2014, 191, 344-350.
15. P. Xie, F. Guo, R. Xia, Y. Wang. *J. Lumin*. 2014, 145, 849–854.
16. J. R. Burdo, J. R. Connor. *BioMetals.* 2003, 16, 63-75.
17. J. An, Z. Yang, M. Yan, T. Li. *J. Lumin.* 2013, 139, 79-83.
18. A. S. Pithadia, M. H. Lim. *Curr. Opin. Chem. Biol.* 2012, 16:67–73.
19. X. Chen, S. Wua, J. Han, S. Han. *Bioorg. Med. Chem. Lett.* 2013, 23, 5295-5299.
20. N. R. Chereddy, K. Suman, P. S. Korrapati, S. Thennarasu, A. B. Mandal, *Dyes and Pig.* 2012, 95, 606-613.
21. J. H. Huang, Y. F. Xu and X. H. Qian Dalton Trans. 2014, 43, 5983–5989.
22. H. Li, L. Li, B. Yin. *Inorg. Chem. Commun.* 2014, 42, 1-4.
23. L. Yang, W. Zhu, M. Fang, Q. Zhang, C. Li. *Spectrochimica Acta, Part A*. 2013. 209. 168-192.
24. P. Danjoua, L. Lyskawa, F. Delattre, M. Becuwe. *Sens. Actuators, B.* 2012, 171, 1022-1028.
25. L. Wang, H. Li, D. Cao. *Sens. Actuators, B*. 2013, 181, 749-755.
26. L. Jiang, L. Wang, B. Zhang, G. Yin, R. Wang. *Eur. J. Inorg. Chem.* 2010, 4438–4443.
27. H. Xiao, K. Chen, N. Jiang, D. Cui, G. Yin, J. Wang, R. Wang. *Analyst.* 2014, 139, 1980–1986.